

# General Approaches to Solving Problems of Analysis and Synthesis of Directional Properties of Antenna Arrays

Islam Islamov, Elmar Humbataliyev

Department of Radio Engineering and Telecommunication, Azerbaijan Technical University, H. Javid ave. 25, AZ1073, Baku, Azerbaijan

Corresponding author: Islam Islamov (e-mail: icislamov@mail.ru).

**ABSTRACT** The work carried out the calculation and synthesis of antenna arrays used in radio-electronic complexes on unmanned aerial vehicles. The analytical model is designed to find asymptotic estimates of the polarization components of the electric field of the grating in the far zone of the carrier surface; the results obtained with its use are the initial data for constructing a technique for the numerical solution of a boundary value problem for a grating on a carrier surface in the CST MWS electrodynamic simulation environment. The synthesis of gratings with the maximum achievable coefficient of directional action is carried out with the control of radiation patterns at a given set of angles. A two-mirror antenna system has been calculated. It is shown that with an increase in the number of re-reflections taken into account, the convergence of the result for the calculated characteristics of the antenna is observed. To test the proposed method, the same antenna was calculated using the integral equation method. The comparison showed a high degree of agreement between the results obtained by two different methods. The results of the simulation based on a software algorithm designed to quantify the input matching at the input of a multichannel frequency-scanning antenna array power divider are presented. It was found that when performing wide-angle scanning in a relative frequency band of more than a few percent, the disadvantage of the known method for eliminating the normal effect is a sharp deterioration in matching in the lower and upper frequencies of the operating range. A new method is proposed based on an automated iterative process of optimizing the divider geometry, which makes it possible to obtain an acceptable match over the entire operating frequency band. The feasibility of switching from a serial power divider construction scheme to a series-parallel scheme is analyzed for wide-angle scanning in a relative frequency band of about 5%.

**INDEX TERMS** Radiation patterns, Antenna arrays, Directional factor, Side lobe level, Surface utilization, Power divider.

## I. INTRODUCTION

Whip antenna arrays, the dimensions of elements that do not exceed the wavelength of the operating range, are used in radio-electronic complexes on unmanned aerial vehicles. According to [1, 2], due to the possibility of matching antenna elements with distribution (feeding) lines in a wide frequency band, due to the absence of sign alternating reactive components of input impedances and significant radiation resistance [3, 4], arrays of this type are used:

- in the means of monitoring the radio-electronic situation for the detection and direction finding of sources of radio emissions;
- in devices for setting deliberate interference to disrupt the stable operation of information and telecommunication systems while maintaining the electromagnetic compatibility of objects not intended for destructive effects;

- in the communication equipment of unmanned aerial vehicles with ground control points for information exchange and transmission of commands to control onboard target loads and their carriers.

Given the low profiles of the structures, pin gratings meet the requirements for the weight and size characteristics of the target loads; when they are placed on the sides, the external appearance, flight performance, and radar signature indicators [5-7] of unmanned aerial vehicles do not change.

At the same time, when designing whip antenna systems, it is necessary to take into account that the type of their radiation patterns and the values of the directivity coefficients significantly depends on the shape, dimensions, and electrical properties of the bearing surfaces [3-5].

Interrelations between the parameters of antenna structures and the objects on which they are located, with indicators of spatial-frequency selectivity of transmission (reception) of radio signals are established based on the

results of electrodynamic analysis based on solving the problems of excitation of receiving-radiating structures by fields (currents) of external sources [8, 9]. When constructing electrodynamic models of antenna systems, carriers are represented by bodies in a simple form with minimal deviations of the coordinate surfaces from the real ones [6]. Rational parameters of antennas and bearing surfaces that provide the required characteristics of the transmission (reception) of wave processes are found by performing the synthesis of receiving and emitting structures by the established criteria [10]. The search for parameters is carried out with a given topology of objects; the choice of the technical appearance of the design of the antenna system from a variety of equivalent alternative options is carried out taking into account the complexity of the technical implementation and the levels of development of production technologies [9].

## II. MATHEMATICAL MODEL AND CALCULATION METHOD

When constructing a mathematical model of the antenna array under study, we will assume that a round cylinder with a cross-sectional radius  $a$  and generatrix length  $h$ , acting as a carrier surface, is located in a homogeneous, isotropic, infinitely extended space. To describe the location of the lattice elements and calculate the surface currents, we set a cylindrical coordinate system in  $(\rho, \varphi, z)$ , which the  $Oz$  axis coincides with the central longitudinal axis of the cylinder. In the interests of reducing the complexity of mathematical transformations without loss of generality of reasoning, we place the point  $O$  at an equal distance from the edges, i.e. planes  $z = \pm h/2$  pass through its ends. To calculate the polarization components of the field, as well as the radiation patterns and the directional action of the grating, we define the spherical coordinate system  $(r, \varphi, \theta)$ , aligning its center with the origin of the cylindrical coordinate system.

The antenna array is a system of  $N$  elementary electric vibrators arranged with a step  $d$ ; the position where the first (closest to one of the ends) an element characterized by coordinates  $(a, 0, l)$ ; distance  $l$  satisfies the following conditions:  $|l| \leq \pm h/2$  and  $|l| \leq h - (N - 1)d$ .

According to [10, 11], the normalized complex radiation pattern of the array has the form

$$\dot{F}(\theta, \varphi) = \sum_{n=1}^N i_n^* f_n(\theta, \varphi), \quad (1)$$

where  $i_n$  is the complex current amplitude of the  $n$ -th antenna element,  $n=1, \dots, N$ ,

$$f_n(\theta, \varphi) = D_n(\theta, \varphi) \exp \left\{ -j \frac{2\pi}{\lambda} (a \cos(\varphi - \varphi_0) \times \right. \\ \left. \times \sin \theta + (l + (n-1)d) \cos \theta) \right\}. \quad (2)$$

- partial diagram of the  $n$ -th vibrator at a wavelength  $\lambda$ ,  $D_n(\theta, \varphi)$  – diffraction factor of the bearing surface, which establishes the patterns of change in the shape of the radiation patterns of the grating (1), located in free space, due

to the induction of surface currents of the cylinder [3, 4], \* - is the sign of complex conjugation. When analyzing a lattice placed in free space, the factor is  $D_n(\theta, \varphi) = 1$ , and the parts diagram (2) takes the form of a complex exponential (at  $\varphi_0 = 0$  and  $l = 0$ ). Based on the definition of the directional patterns of the array (1), the expression for the directional coefficient determines the degree of excess of the power of the emitted (received) electromagnetic field over the level characteristic of a hypothetical isotropic antenna [9], can be represented as

$$G(\theta, \varphi) = 4\pi \left\{ \sum_{n=1}^N \sum_{p=1}^N i_n^* C_p(\theta, \varphi) i_p \right\} \cdot \left\{ \sum_{n=1}^N \sum_{p=1}^N i_n^* S_p i_p \right\}^{-1}, \quad (3)$$

where

$$C_p(\theta, \varphi) = f_n(\theta, \varphi) f_p(\theta, \varphi), n, p = 1, \dots, N, \quad (4)$$

- are the space-energy coefficients of the electromagnetic interaction of the  $n$ -th and  $p$ -th antenna elements [11],

$$S_p = \int_0^{2\pi} \int_0^\pi f_n(\theta, \varphi) f_p(\theta, \varphi) \sin \theta d\theta d\varphi, n, p = 1, \dots, N, \quad (5)$$

- is an expression for calculating the power of the field emitted (received) by a hypothetical isotropic antenna, according to the level at which the power of the array field changes from the radiation patterns (1).

Using the method of induced currents [8] to calculate the diffraction factor, we write down the asymptotic estimates of the polarization components of the grating electric field in the far zone of the carrier surface [12-16].

$$\dot{E}_\theta(r, \theta, \varphi) = -j \frac{\exp\left(-j \frac{2\pi r}{\lambda}\right)}{2r\lambda} \times \\ \times \left\{ \mu_0 c \sum_{n=1}^N M_{\theta n}(\theta, \varphi) + \sum_{n=1}^N L_{\varphi n}(\theta, \varphi) \right\}, \quad (6)$$

$$\dot{E}_\varphi(r, \theta, \varphi) = -j \frac{\exp\left(-j \frac{2\pi r}{\lambda}\right)}{2r\lambda} \times \\ \times \left\{ \mu_0 c \sum_{n=1}^N M_{\varphi n}(\theta, \varphi) + \sum_{n=1}^N L_{\theta n}(\theta, \varphi) \right\}, \quad (7)$$

where

$$\begin{bmatrix} M_{\theta(\varphi)n}(\theta, \varphi) \\ L_{\theta(\varphi)n}(\theta, \varphi) \end{bmatrix} = \begin{bmatrix} M_{\theta(\varphi)}(\theta, \varphi) \\ L_{\theta(\varphi)}(\theta, \varphi) \end{bmatrix} \times \\ \times \exp \left\{ -j \frac{2\pi}{\lambda} (a \cos(\varphi - \varphi_0) \sin \theta + \right. \\ \left. + (l + (n-1)d) \cos \theta) \right\}, \quad (8)$$

- local diffraction functions characterizing the change in the field distribution of the  $n$ -th vibrator,  $n=1, \dots, N$ , due to scattering on the carrier surface

$$\begin{bmatrix} M_\theta(\theta, \varphi) \\ L_\theta(\theta, \varphi) \end{bmatrix} = a \sin \theta \int_0^{2\pi} \int_{-h/2}^{h/2} \begin{bmatrix} H_\varphi(a, \varphi', z') \\ -E_\varphi(a, \varphi', z') \end{bmatrix} \times \\ \times \exp \left\{ -j \frac{2\pi}{\lambda} (a \cos(\varphi - \varphi') \sin \theta + z' \cos \theta) \right\} dz' d\varphi', \quad (9)$$

$$\begin{bmatrix} M_\varphi(\theta, \varphi) \\ L_\varphi(\theta, \varphi) \end{bmatrix} = a \int_0^{2\pi} \int_{-h/2}^{h/2} \begin{bmatrix} -H_z(a, \varphi', z') \\ E_z(a, \varphi', z') \end{bmatrix} \times \exp\left\{j \frac{2\pi}{\lambda} (a \cos(\varphi - \varphi') \sin \theta + z' \cos \theta)\right\} dz' d\varphi', \quad (10)$$

- are the diffraction functions of the magnetic and electric fields of the cylinder [17],  $H_{\varphi(z)}(r', \varphi', z')$  and  $E_{\varphi(z)}(r', \varphi', z')$  – are the components of the magnetic and electric fields on the surface of  $r' = a$  an infinitely extended cylinder,  $\mu_0$  – magnetic permeability of free space,  $c$  is the speed of light.

To calculate definite integrals in (9) and (10), we use the principle of equivalence of fields and surface currents induced by them and the method developed in [18] for approximating the currents of objects with axial symmetry by a series of cylindrical functions. In this case, the diffraction functions of the cylinder fields (9) and (10) are calculated in an analytical form, and the local diffraction functions of sources located at the points of attachment of the array elements on the carrier surface are found by summing the series of trigonometric functions of azimuthal harmonics [18] with weight coefficients in the form relations of the Hankel functions.

As a result of these procedures, from (2) and (6)-(10) we obtain

$$D_n(\theta, \varphi) = \sqrt{D_{n\theta}^2(\theta, \varphi) + D_{n\varphi}^2(\theta, \varphi)}, n=1, \dots, N, \quad (11)$$

where

$$D_{n\theta}(\theta, \varphi) = \frac{2\pi\mu_0 l_0 a}{\lambda^2} \times \left\{ 2 \cos \theta \cos \varphi \exp\left(j \frac{2\pi}{\lambda} \sin \theta \cos \varphi\right) - \sum_{m=0}^{\infty} \varepsilon_m j^m \cos(m\varphi) \gamma_{nm}^\theta \right\}, \quad (12)$$

$$D_{n\varphi}(\theta, \varphi) = -\frac{2\pi\mu_0 l_0 a}{\lambda^2} \times \left\{ 2 \sin \varphi \exp\left(j \frac{2\pi}{\lambda} \sin \theta \cos \varphi\right) - \sum_{m=1}^{\infty} j^m \sin(m\varphi) \gamma_{nm}^\varphi \right\}, \quad (13)$$

- are the azimuthal and axial components of the diffraction factor of the cylinder [19-22] for the  $n$ th array element,  $n=1, \dots, N$ ,  $l_0$  is the length of the electric dipole,

$$\varepsilon_m = \begin{cases} 1, & m = 0, \\ 2, & m \neq 0. \end{cases}$$

The coefficients  $\gamma_{nm}^\theta, m \geq 0$ , and  $\gamma_{nm}^\varphi, m \geq 1$ , included in (12) and (13) are calculated according to the rules [8]

$$\gamma_{nm}^\theta = \int_{-\infty}^{\infty} k \left\{ \frac{\dot{H}_m^{(2)}\left(\frac{2\pi a}{\lambda} \alpha\right)}{H_m^{(2)}\left(\frac{2\pi a}{\lambda} \alpha\right)} - \left(\frac{m\lambda}{2\pi a}\right)^2 \frac{H_m^{(2)}\left(\frac{2\pi a}{\lambda} \alpha\right)}{\dot{H}_m^{(2)}\left(\frac{2\pi a}{\lambda} \alpha\right)} \right\} \times \exp\left\{j \frac{2\pi}{\lambda} (h - (l + (n-1)d))(\cos \theta - k)\right\} \frac{dk}{\cos \theta - k} \quad (14)$$

$$\times \left( - \exp\left\{-j \frac{2\pi}{\lambda} \left(\frac{h}{2} - (l + (n-1)d)\right)(\cos \theta - k)\right\} \right) dk, \\ \gamma_{nm}^\varphi = \int_{-\infty}^{\infty} \frac{H_m^{(2)}\left(\frac{2\pi a}{\lambda} \alpha\right)}{-\alpha \dot{H}_m^{(2)}\left(\frac{2\pi a}{\lambda} \alpha\right)} \times \exp\left\{j \frac{2\pi}{\lambda} (h - (l + (n-1)d))(\cos \theta - k)\right\} \frac{dk}{\cos \theta - k} \quad (15) \\ \times \left( - \exp\left\{-j \frac{2\pi}{\lambda} \left(\frac{h}{2} - (l + (n-1)d)\right)(\cos \theta - k)\right\} \right) dk,$$

where  $\alpha = \sqrt{1 - k^2}$  – is the longitudinal wavenumber [20],  $H_m^{(2)}(\dots)$  – is the Hankel function of the second kind of the

$m$ -th order,  $\dot{H}_m^{(2)}\left(\frac{2\pi a}{\lambda} \alpha\right)$  – is its derivative concerning the variable  $r$  at the point  $r = a$ .

Thus, expressions (1), (2) and (11)-(15) make it possible to analyze the radiation patterns of an array of electric vibrators on the side surface of a perfectly conducting cylinder of finite length. When expressions (3)-(5) are used together, taking into account (2) and (11)-(15), relationships can be established between the grating directivity factor and its design parameters and cylinder dimensions.

### III. A METHOD FOR SYNTHESIZING AN ANTENNA ARRAY WITH A MAXIMUM DIRECTIVITY FACTOR WITH RESTRICTIONS ON THE SHAPE OF THE RADIATION PATTERNS

In the presented work, based on the method of indefinite Lagrange multipliers, the synthesis of an antenna array was performed according to the criterion of maximizing the directional coefficient when forming nulls of the radiation patterns in fixed directions. In this case, unlike [9, 11], the single Lagrange multiplier, which minimizes the integral difference between the initial and required radiation patterns in the circular sector of angles [10], is replaced by a set of Lagrange multipliers for  $Q \leq N - 1$  directions  $(\theta_q, \varphi_q), q = 1, \dots, Q$ .

Using the definition of radiation patterns  $F(\theta, \varphi) = |\dot{F}(\theta, \varphi)|$ , in which the levels  $\alpha_q$  are controlled at  $(\theta_q, \varphi_q), q = 1, \dots, Q$ , and expression (3) to calculate the directional effect of the array, taking into account (2), (4) and

(5), by analogy with the synthesis criterion [20], we define the system of equations

$$\begin{cases} G(\theta_0, \varphi_0) \rightarrow \max \\ F(\theta_q, \varphi_q) = \alpha_q, q = 1, \dots, Q, Q \leq N - 1. \end{cases} \quad (16)$$

According to the method of indefinite Lagrange multipliers, the currents of the antenna elements  $i_n, n = 1, \dots, N$ , in (1) and (3), ensuring the achievement of the maximum directivity at  $Q$  fixed levels of the array radiation patterns, satisfy the parametric distribution corresponding to the minimum of the functional

$$T = \sum_{n=1}^N \sum_{p=1}^N i_n^* S_p i_p + \sum_{q=0}^Q \lambda_q \sum_{n=1}^N f_n(\theta_q, \varphi_q) i_n^*, \quad (17)$$

where  $\lambda_q$  are indefinite Lagrange multipliers,  $q = 1, \dots, Q$ , acting as parameters of complex current amplitudes.

Calculating the first derivative of the functional (17) concerning the components of the column vector  $i_n, n = 1, \dots, N$ , and equating it to zero, we obtain a system of linear algebraic equations concerning the desired distribution of grid currents

$$i_n = - \sum_{q=0}^Q \lambda_q^* \sum_{p=1}^N S_p^{-1} f_p(\theta_q, \varphi_q), \quad (18)$$

where  $S_p^{-1}$  – are elements of the matrix inverse  $S_p, n, p = 1, \dots, N$ .

The indefinite Lagrange multipliers included in (18) are the roots of the system of linear algebraic equations formed as a result of substituting the current distribution (18) into (1), and the resulting expression into the second equation of the system (16).

$$\begin{aligned} \sum_{s=0}^Q \lambda_q^* \sum_{n=1}^N \sum_{p=1}^N f_n(\theta_q, \varphi_q) S_p^{-1} f_p(\theta_s, \varphi_s) = \\ = -\alpha_q, q = 0, \dots, Q. \end{aligned} \quad (19)$$

The solution of the resulting system of equations was found using the simplex method when converting the invertible matrix on the left side of (19) to the canonical form with the choice of the largest coefficient in absolute value. Antenna element currents satisfying distribution (18) with Lagrange multipliers converting equations of system (19) into identities. Due to the performed transformations, it became possible to correct the amplitudes and phases of the currents of each vibrator. An electrodynamic simulation was carried out in the CST MWS environment.

The radiation patterns of a linear array of  $N = 5$  vibrators with a height of  $l_0 / \lambda = 0,2$  are calculated, located with a step  $d / \lambda = 0,25$  on a cylinder with a normalized length  $h / \lambda = 5$  and an electric radius  $a / \lambda = 0,3$ . The calculation results are shown in Fig. 1, a. Fig. 1, b shows the radiation pattern of the same grating when zero is formed with a depth of 20 dB according to criterion (16).

From a comparison of the presented results, it follows that in the direction of the local maximum of the radiation patterns in Fig. 1, a, a deep extremum of the radiation patterns in Fig. 1, b is created with an increase in the back

lobe. In Figure 2, solid lines show the radiation patterns of arrays of  $N = 5$  (Fig. 2, a) and  $N = 7$  vibrators (Fig. 2, b) with directivity of 7,4 dB and 9,2 dB, respectively; the dotted line shows the radiation patterns with synthesized nulls. For an array of  $N = 5$  elements, zero was obtained in the direction of 180°, and the minimum values of the radiation patterns fall on a sector of angles with a width of about 60°; the directional coefficient reaches a value of 6,2 dB, the increase in the rear lobe does not exceed 2 dB. For an array of  $N = 7$  elements, the zero of the radiation patterns was formed in the direction of 135°; at the same time, the sectoral failure of radiation patterns with an angular width of 10° with a decrease in the directivity to 8,1 dB.

To assess the possibilities of increasing the directivity of antenna arrays with the formed zeros of the radiation patterns, cyclic multiple corrections of the distributions of the amplitudes and phases of the currents on the vibrators were carried out.

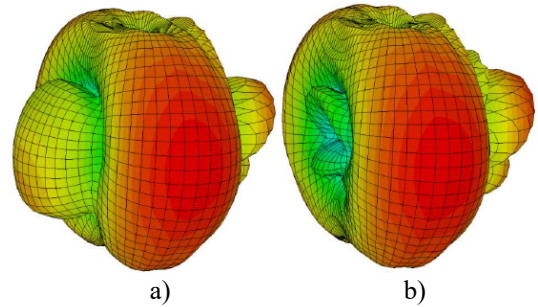


FIGURE 1. Normalized radiation patterns of an antenna array of  $N = 5$  elements without specially created zeros (a) and with one generated synthesized (b).

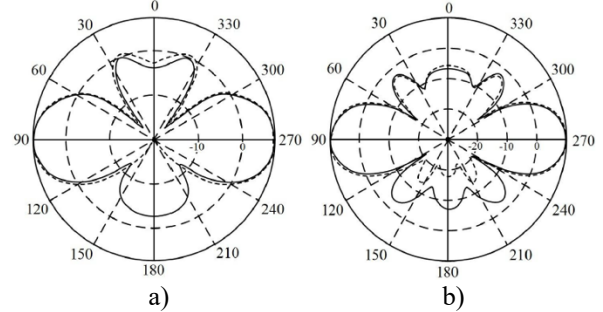


FIGURE 2. Normalized radiation patterns of antenna arrays of  $N = 5$  (a) and  $N = 7$  elements (b) without specially created zeros (solid lines) and with zeros formed according to criterion (16).

By adjusting the directivity of the array of  $N = 5$  elements, it increased from 7,4 dB to 7,5 dB due to the narrowing of the main beam and reduction of the angular sector, where the depth of extremes does not exceed - 20 dB, from 60° to 35° when performing requirements for radiation patterns established by the second equation of system (16). For an array of  $N = 7$  elements, it was found that with a practically unchanged directivity factor (9,2 dB), due to diffraction distortion of currents at the points of attachment of the vibrators on the carrier surface, the sector dip of the directivity patterns narrows from 10° to 5°.

#### IV. ANTENNA SYSTEM CALCULATION

Fig. 3, 4, and 5 show the calculated directivity in the range of angles at frequencies  $f = 1,7 \text{ GHz}$ ,  $3,4 \text{ GHz}$ , and  $5,1 \text{ GHz}$ , respectively (we compared the calculation by the method of physical optics (MPO) and the calculation by the method of integral equations). It is easy to see that there is almost a complete coincidence between the directional coefficient in the region of the main lobe and the first side lobe. The successful result of comparing the characteristics of a two-mirror antenna obtained by different methods allows us to conclude that the MPO, taking into account re-reflections, is suitable and highly accurate for the problem under consideration.

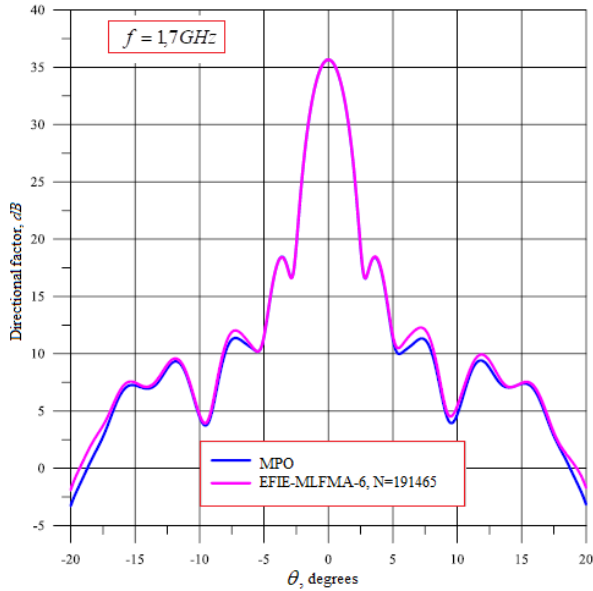


FIGURE 3. Estimated directivity at  $f = 1,7 \text{ GHz}$ .

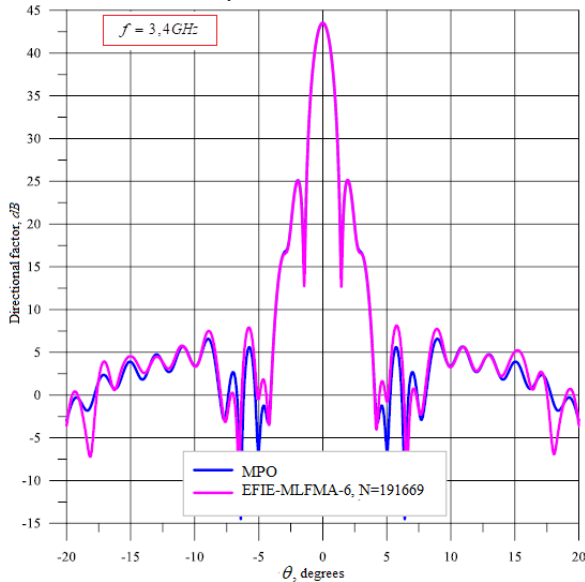


FIGURE 4. Estimated directivity at  $f = 3,4 \text{ GHz}$ .

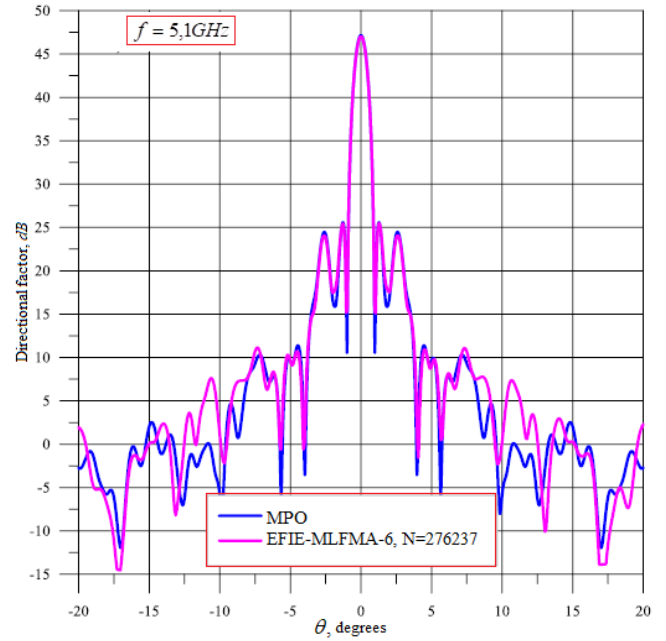


FIGURE 5. Estimated directivity at  $f = 5,1 \text{ GHz}$ .

Fig. 6 shows the design gain of the antenna at maximum radiation patterns in the frequency range from 1 to 10 GHz. It is easy to see that there are oscillations on the curve that violate the monotonic growth with increasing frequency.

Fig. 7 shows the corresponding calculated antenna surface utilization factor in the frequency range from 1 to 10 GHz. On the surface utilization curve, oscillations are more pronounced, have a maximum amplitude at the left edge of the operating range, and gradually decay with increasing frequency. Fig. 8 shows the calculated surface utilization of a two-mirror antenna in a narrow frequency range from 1,4 to 1,9 GHz. According to the graph, we determine that the oscillation period here is  $\approx 90 \text{ MHz}$ .

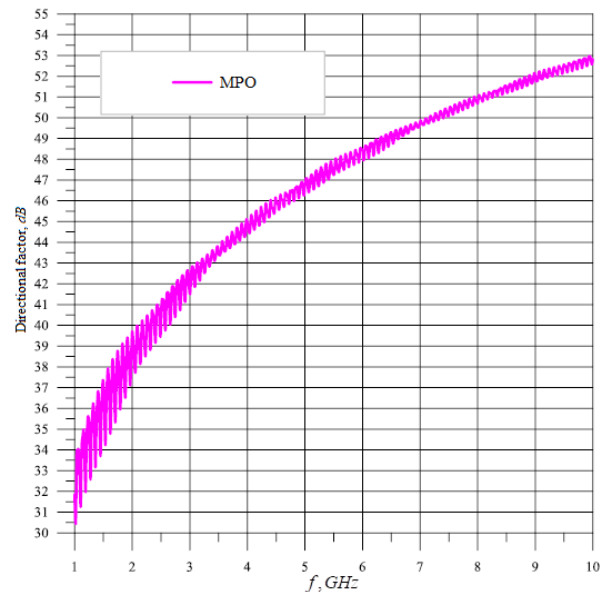


FIGURE 6. Estimated directivity in the frequency range from 1 to 10 GHz.

The calculation by the MPO showed that in this case the oscillations practically disappear, and in the entire frequency range there is a surface utilization factor of approximately 0,7. The physical reason for the presence of oscillations in the antenna surface utilization factor in the frequency range is a change in the amplitude-phase distribution of the electric current on the main mirror due to multiple reflections in the open mirror resonator. At the right end of the frequency range, multipath fades quickly and has less effect on antenna performance.

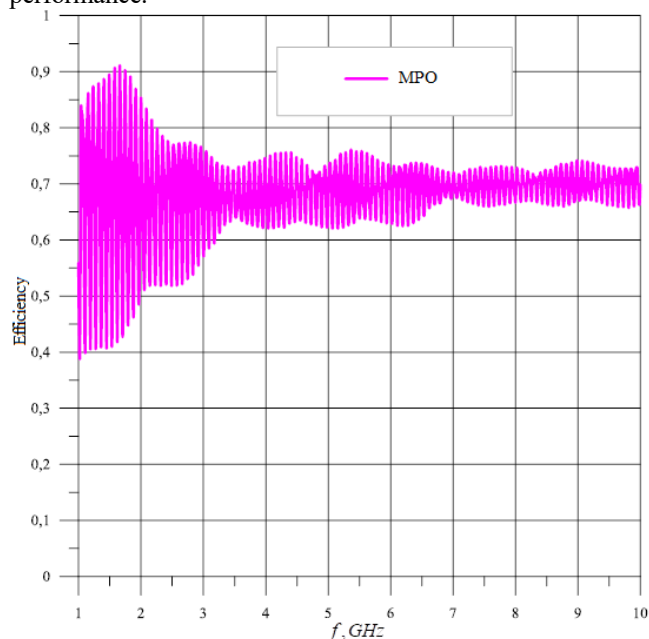


FIGURE 7. Estimated surface utilization factor in the frequency range from 1 to 10 GHz.

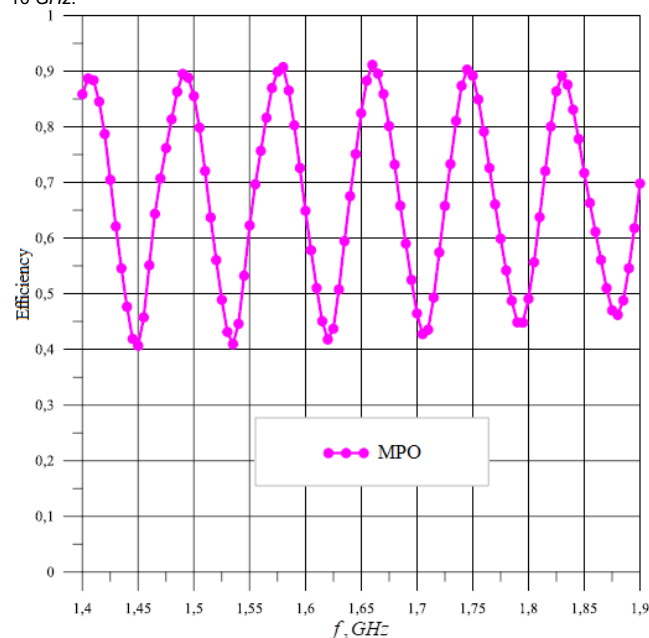


FIGURE 8. Estimated surface utilization factor in the frequency range from 1,4 to 1,9 GHz.

## V. SIMULATION OF AN ANTENNA DEVICE WITH FREQUENCY SCANNING

The work carried frequency scanning antenna arrays, widely used in airspace surveillance and air traffic control radar systems, in most cases represent a flat equidistant array of linear radiators connected to a multichannel traveling wave power divider based on couplers that are connected in series to the sinusoidal delay line. configurations [23]. It is known that a significant disadvantage of such antennas is a sharp increase in the voltage standing wave ratio at the input of the power divider at a frequency corresponding to the formation of a radiation pattern beam in the direction of the normal to the radiating aperture, as a result of in-phase addition of a large number of even small reflections from periodic inhomogeneities - bends delay lines and taps. This phenomenon, which leads to a significant loss of gain and unacceptable distortion of the shape of the radiation pattern, is called the “normal effect” in the literature [24]. At present, the most widely used method is to eliminate the normal effect, based on the displacement of even and odd groups of periodic inhomogeneities of the power divider relative to each other by an odd integer number of quarters of the wavelength in the delay line [25]. However, the results of experimental tests of the characteristics of antenna arrays with frequency scanning, in which this method is implemented [26], show that when wide-angle scanning is carried out in a relative band of more than a few percent, there is a sharp deterioration in matching in the lower and upper frequencies of the operating range.

This paper describes an algorithm for analyzing the frequency response of the standing wave ratio concerning the voltage at the input of a multi-element antenna array with frequency scanning at a known level of reflections from periodic inhomogeneities of the power divider, taking into account the amplitude-phase distribution formed in the frequency scanning plane.

The work aim to simulate the effect of the normal in an antenna array with frequency scanning, to find effective ways to eliminate this phenomenon based on the proposed algorithm.

## VI. DESCRIPTION OF THE ALGORITHM

The studied model of the antenna array with frequency scanning, shown in Fig. 9 is a flat equidistant array of linear emitters ( $R_1, R_2, \dots, R_N$ ) separated by a distance  $d$  and excited from input 1 using a series power supply system - a multichannel traveling wave power divider, which is built based on power couplers 3 included in the delay line sinusoidal configuration 2. Power is removed from the delay line at regular intervals having a length  $S$  (delay line period). The output of the delay line, if necessary [27], is matched with an absorbing load 4.

It is known that the position of the directional pattern beam  $\theta$  in space depends on the phase relations of electrical oscillations in the emitters and (if we denote the wavelength in free space by  $\lambda$ , and the wavelength in delay line by  $\lambda_g$ ) is determined based on the following equation [28-30]:

$$\frac{2\pi}{\lambda} d \sin \theta = \frac{2\pi}{\lambda_g} S - 2\pi i, \quad (20)$$

where  $i$  is an integer. Respectively,

$$\theta = \arcsin \left[ \frac{S\lambda}{d} \left( \frac{1}{\lambda_g} - \frac{i}{S} \right) \right]. \quad (21)$$

The algorithm for quantitative estimation of the frequency response of the standing wave ratio by the voltage at input 1 of the antenna array with frequency scanning is implemented based on the following relations, intended for the analytical description of the design parameters and electrical characteristics of the model (Fig. 9).

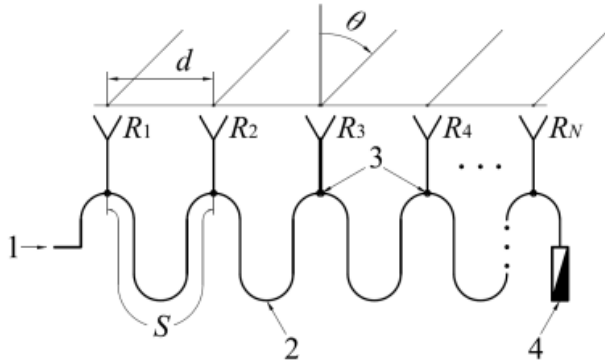


FIGURE 9. Structural diagram of a frequency-scanning antenna array with serially fed emitters.

The investigated frequency ranges in the discrete form:

$$f_m - f_l + \frac{f_h - f_l}{M - 1} (m - 1), \quad (22)$$

where  $f_l$  and  $f_h$  are, respectively, the extreme lower and upper frequencies of the studied range;  $M$  is the number of frequency points in the range;  $m = 1, 2, \dots, M$ .

Delay line period length:

$$S = \lambda_{gn} n_\lambda, \quad (23)$$

where  $\lambda_{gn}$  is the wavelength in the delay line at the frequency  $f_n$  (normal frequency) corresponding to beam formation of the radiation patterns in the direction normal to the antenna array aperture, i.e. at  $\theta = 0^\circ$ ;  $n_\lambda$  is the number of wavelengths at the frequency of the normal  $\lambda_{gn}$ , forming one period of the delay line.

Amplitude distribution formed at the outputs of the power divider:

$$A_n = p + (1 - p) \cos(\pi X_n)^g, \quad (24)$$

where  $N$  is the number of outputs of the power divider;

$n = 1, 2, \dots, N$ ;  $X_n = \frac{n-1}{N-1} - \frac{1}{2}$ ;  $p$  and  $g$  are variable coefficients that determine the shape of the amplitude distribution.

Normalized power distribution formed at the outputs of the power divider:

$$P_n = \frac{A_n^2}{\sum_{n=1}^N A_n^2}. \quad (25)$$

Power propagating in the  $n$ th period of the delay line:

$$Pd_n = (Pd_{n-1} - P_n) 10^{\frac{\alpha s}{10}}, \quad (26)$$

where  $n = 2, 3, \dots, N$ ;  $Pd_1 = (1 - P_1) 10^{\frac{\alpha s}{10}}$  – power propagating in the 1st delay line period after the 1st coupler;  $\alpha s = \alpha S$  – power loss in one period of the delay line;  $\alpha$  – loss per unit length in delay lines in dB/m.

Coupling coefficients of the power divider couplers from the delay line:

$$Cf_n = 10 \lg \left( \frac{P_n \eta}{Pd_{n-1}} \right), \quad (27)$$

where  $n = 2, 3, \dots, N$ ;  $Cf_1 = 10 \lg(P_1 \eta)$  – coupling coefficient of the 1st coupler of the power divider with delay lines;  $\eta$  – efficiency, determined by the power loss in the power divider. In the absence of an absorbing load in the power divider  $Cf_N = 0 \text{ dB}$ .

The amplitude of the reflection coefficient from the  $n$ -th periodic inhomogeneity of the power divider:

$$|Q_n| = \frac{R_n - 1}{R_n + 1}, \quad (28)$$

where  $R_n$  is the voltage standing wave ratio of the  $n$ -th periodic inhomogeneity, for power couplers  $R_n = Rc_n$ , and for delay line bends  $R_n = Rb_n$ .

Power propagating in the  $n$ -th period of the power divider delay line:

$$Pt_n = Pt_{n-1} \left( 1 - 10^{\frac{Cf_{n-1}}{10}} \right) 10^{\frac{\alpha s}{10}}, \quad (29)$$

where  $n = 2, 3, \dots, N$ ;  $Pt_1 = 1$  – power at the input of 1 power divider.

Power reflected from the  $n$ -th periodic inhomogeneity of the power divider:

$$Ph_n = Pt_n |Q_n|^2. \quad (30)$$

The power reflected from the  $n$ -th periodic inhomogeneity and arrived at the input of 1 power divider (taking into account the attenuation when passing through the couplers during backpropagation):

$$Pe_n = Ph_n \left( 1 - \sum_{n=1}^{n-1} 10^{\frac{Cf_{n-1}}{10}} \right) 10^{\frac{\alpha s(n-1)}{10}}, \quad (31)$$

where  $n = 2, 3, \dots, N$ ;  $Pe_1 = Ph_1$  power reflected from the 1st inhomogeneity.

The phase of the reflection coefficient from the  $n$ -th periodic inhomogeneity de:

$$\arg(Q_{m,n}) = -\frac{4\pi}{\lambda_{gm}} S(n-1) + \varphi_0, \quad (32)$$

where  $\lambda_{gm}$  is the wavelength in the delay lines corresponding to the  $m$ -th frequency point  $f_m$  of the studied range  $\varphi_0$  and is the initial phase of the reflection coefficient.

By the principle of superposition, the total reflection coefficient at the input 1 of the antenna array power divider at the  $m$ -th frequency point:

$$Q_{1m} = \sum_{n=1}^N \left[ \sqrt{P e_n} e^{j \arg(Q_{m,n})} \right] \quad (33)$$

where  $j = \sqrt{-1}$ .

The standing wave ratio for voltage at the input of 1 power divider at the  $m$ -th frequency point:

$$VSWR_m = \frac{1 + |Q_{1m}|}{1 - |Q_{1m}|} \quad (34)$$

Thus, using the operating frequency range, the level of reflections from periodic inhomogeneities, and the amplitude-phase distribution formed in the frequency scanning plane with a known delay line configuration as initial data, a calculation estimate of the standing wave coefficient from the voltage at the input of a multielement antenna array can be made.

## VII. SIMULATION RESULTS

The simulation was carried out based on developed and experimentally studied prototypes of a single-channel  $S$ -band antenna array, which preceded the creation of a monopulse antenna [31-34]. These antenna arrays are a flat equidistant array of linear radiators (rows) installed with a pitch of  $d = 70 \text{ mm}$  and connected to a 54-channel waveguide power divider built based on 53  $T$ -slot directional couplers connected in series in the delay lines [35-38]. In this case, the final load of the delay line is the last emitter  $R_{54}$ . The scanning sector of the antenna array in the vertical plane in the operating frequency range is  $50^\circ$ .

The chosen option for constructing a power divider makes it possible to perform simulation without taking into account the final level of radiator matching [39] since the main part of the power reflected from the radiators is dissipated in the balanced loads of the directional coupler.

The simulation was performed taking into account the following initial data: operating frequency range of the antenna: from  $2,7 \text{ GHz}$  to  $2,85 \text{ GHz}$  ( $5,4\%$ ); number of power divider outputs:  $N = 54$ ; analyzed frequency range:  $f_i = 2,68 \text{ GHz}$ ,  $f_h = 2,87 \text{ GHz}$ ,  $M = 1901$ ; normal frequency:  $f_n = 2,77 \text{ GHz}$ ; type of delay line waveguide: rectangular (section  $a \times b = 62,4 \times 17 \text{ mm}$ ); linear losses in delay lines:  $\alpha = 0,07 \text{ dB/m}$ ; the number of wavelengths at the frequency of the normal forming the period of the delay line:  $n_i = 2,5$ ; coefficients that determine the shape of the antenna array:  $p = 0,19$ ,  $g = 1,65$ ; efficiency of the power divider:  $\eta = 79\%$ ; standing wave coefficient for the voltage of the bends of the delay line ( $Rb_n$ ): distributed according to a random uniform law in the range from  $1,02$  to  $1,04$ ; standing wave ratio for the voltage of the directional coupler ( $Rc_n$ ): distributed according to a random uniform law in the range from  $1,05$  to  $1,07$ ; the initial phase of the reflection coefficient  $\varphi_0$ : distributed according to a random uniform law in the range from  $170^\circ$  to  $190^\circ$ .

According to the principle of superposition, the resulting voltage standing wave ratio at the input of the antenna array at the  $m$ -th frequency point can be calculated by the formula:

$$VSWR_m = \frac{1 + |Qc_{1m} + Qb_{1m} e^{j\Delta\varphi_m}|}{1 - |Qc_{1m} + Qb_{1m} e^{j\Delta\varphi_m}|}, \quad (35)$$

where  $Qc_{1m}$  - calculated by expression (34) the total reflection coefficient at the input 1 from the directional coupler, similarly  $Qb_{1m}$  - the total reflection coefficient from the bends of the delay line,  $\Delta\varphi_m$  - the phase difference due to the physical separation  $\Delta S$  of the places of reflections from the directional coupler and bends delay lines.

$$\Delta\varphi_m = -\frac{4\pi}{\lambda g_m} \Delta S. \quad (36)$$

The calculation of the standing wave coefficient from the voltage at the input of the antenna array by the algorithm presented above was carried out in two stages. In the first stage, simulation modeling was carried out for 3 variants of the location of periodic inhomogeneities in the power divider considered in [36] (Fig. 10).

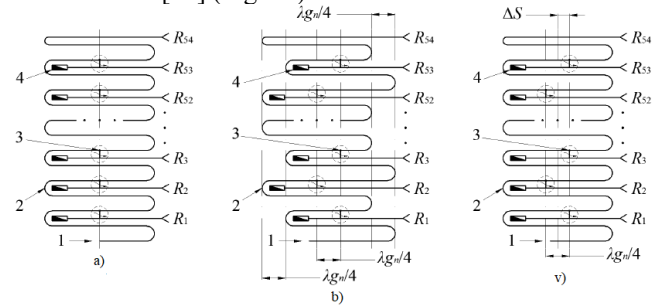


**FIGURE 10.** Variants of the location of periodic inhomogeneities in the power divider: a) there is no shift between even and odd periodic inhomogeneities; b) even and odd periodic inhomogeneities are spaced relative to each other by  $\lambda g_n/4$ ; v) even and odd directional couplers are spaced relative to each other by  $\lambda g_n/4$ , there is no shift between the even and odd bends of the delay line; 1 - input of the antenna array; 2 - sinusoidal delay lines; 3 - directional coupler; 4 - balanced load directional coupler.

Fig. 11 shows typical implementations of the frequency characteristics of the standing wave ratio for the voltage at the input of the antenna array modeled by the given initial data for the cases of Fig. 10, a (red curves) and Fig. 10, b (blue curves). A typical implementation of the frequency response of the voltage standing wave ratio for the case of Fig. 10, is shown in Fig. 12.

An analysis of the obtained results shows that in the absence of a shift between even and odd groups of periodic inhomogeneities (Fig. 11, red curves), there is a sharp increase in the standing wave coefficient for voltage at the input of the antenna array at the frequency of the normal  $f_n$  as a result of the in-phase summation of a large number of reflections delay line bends and directional coupler. When the even and odd groups of periodic inhomogeneities of the power divider are displaced relative to each other by a distance  $\lambda g_n/4$  (by the method of eliminating the normal effect presented in [37]), at the normal frequency  $f_n$ , the reflections from the even and odd groups of the directional coupler cancel each other out and delay line bends due to their antiphase addition at the input of the antenna array (Fig. 11, blue curves). However, due to the dispersion properties

of the delay line, the reflections in the low and high frequencies are added almost in phase, which leads to an unacceptable increase in the voltage standing wave ratio at the edges of the operating range. Under conditions of displacement of even and odd groups of the directional coupler relative to each other by  $\lambda g_n/4$  in the absence of separation between the bends of the delay line, voltage standing-wave coefficient surges are observed both at the normal frequency  $f_n$  and in the lower and upper frequencies of the operating range (Fig. 12). Based on the results obtained, it can be concluded that the recommendations given in the literature on eliminating the effect of the normal in the antenna array, when performing wide-angle scanning in a relative frequency band of more than a few percent, cannot always be successfully applied in the practical implementation of antennas.

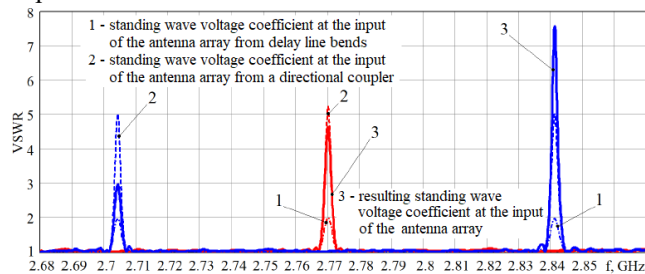


**FIGURE 11.** In a typical implementations of the frequency characteristics of the standing wave ratio for voltage at the input of the antenna array.

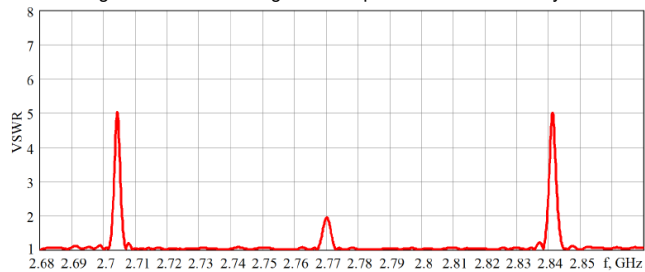


**FIGURE 12.** In a typical implementation of the frequency response of the standing wave ratio for voltage at the input of the antenna array with a shift of even and odd groups of directional couplers relative to each other by  $\lambda g_n/4$ , there is no shift between the even and odd bends of the delay line.

In the second stage of modeling, to eliminate the identified shortcomings in the construction of the antenna array by the options shown in Fig. 10, a new method is proposed based on an automated iterative process of power divider geometry optimization. The essence of the method lies in the violation of the periodicity of the power divider structure due to the displacement of each  $n$ -th directional coupler and the bending of the delay line relative to the center line of the divider (Fig. 10, a) by distances  $\Delta S b_n$  and  $\Delta S c_n$ , respectively, changing from period to period according to a certain law, at which the minimum achievable level of the standing wave ratio for the voltage at the input of the antenna array in the analyzed frequency range is provided. In this case, the phase of the reflection coefficient from the  $n$ -th directional coupler (delay line bend), taking into account expression (32), can be written as:

$$\arg(Q_{m,n}) = -\frac{4\pi}{\lambda g_m} [S(n-1) + \Delta S b(c)_n] + \varphi_0. \quad (37)$$

Consider the process of optimizing the geometry of the power divider. At the first iteration, using the built-in software functions, a data file is written with a certain number (usually from 100 to 500) of realizations of the values  $\Delta S b_n$  and  $\Delta S c_n$ , distributed in the  $n$ th period of the delay line according to a random uniform law in the interval  $\pm \lambda g_n/4$ , and also corresponding to each implementation, calculated taking into account expression (34), the maximum level of the standing wave ratio for voltage from the directional coupler and bends of the delay line at the input of the antenna array.

Then, the recorded data file is analyzed to select the minimum recorded values of the voltage standing wave coefficient and the corresponding realizations of the values  $\Delta S b_n$  and  $\Delta S c_n$ , which for the first iteration are denoted as  $\Delta S b_{1n}$  and  $\Delta S c_{1n}$ . At the second iteration, implementations for  $\Delta S b_n = \Delta S b_{1n} + r b_{1n}$  and  $\Delta S c_n = \Delta S c_{1n} + r c_{1n}$  and the maximum voltage standing wave ratio level corresponding to each of them are added to the data file. In this case, the quantities  $r b_{1n}$  and  $r c_{1n}$  are distributed according to a random uniform law in the reduced interval  $\pm \lambda g_n/8$ . Next, the selection of the minimum fixed values of the voltage standing wave coefficient and the corresponding realizations of the values  $\Delta S b_n$  and  $\Delta S c_n$ , which are designated as  $\Delta S b_{2n}$  and  $\Delta S c_{2n}$  at the second iteration, is also performed. Further, 5 more iterations are performed similarly with a twofold reduction at each subsequent iteration of the distribution interval of the values  $r b_{2n}, r b_{3n}, \dots, r b_{6n}$ , and  $r c_{2n}, r c_{3n}, \dots, r c_{6n}$  to  $\pm \lambda g_n/256$ . At each iteration, the selected realizations  $\Delta S b_n$  and  $\Delta S c_n$  are normalized (if they go beyond the range of  $\pm \lambda g_n/4$ ) by adding to the value of  $\pm \lambda g_n/2$ . After the 7th iteration, a change in the maximum level of the voltage standing wave ratio is observed only in the 3rd and 4th decimal places, while it is obvious that the iterative process of optimizing the geometry of the power divider converged.

Based on the proposed method, as well as the above initial data, the geometry of the power divider was optimized (Fig. 10, a), according to the results of which the displacements  $\Delta S b_n$  and  $\Delta S c_n$  (Fig. 13) were found relative to the axial line of the divider for each  $n$ -th directional coupler and bending of the delay line. The block diagram of the antenna array with the optimized geometry of the power divider is shown in Fig. 14, where 1 is the input, 2 are the delay lines, 3 is the directional coupler, and 4 is the center line of the divider. The frequency characteristics of the standing wave ratio for the voltage at the input of the antenna array, calculated by expressions (34) and (35), taking into account (37), are shown in Fig. 15.

Analyzing the obtained results, we can conclude that the presented method, with a slight increase in the average level of the standing wave ratio for voltage, eliminates the normal effect and provides acceptable matching in the entire operating frequency band of the antenna.

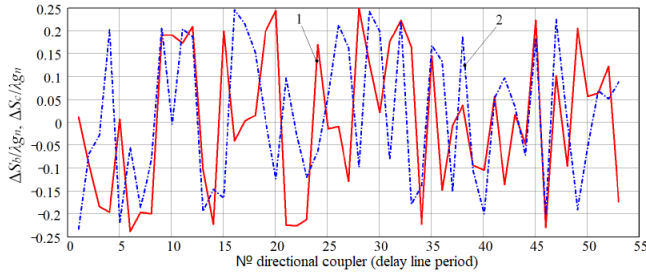


**FIGURE 13.** Offsets of the bends of the delay line (1) and directional coupler (2) relative to the center line of the power divider.

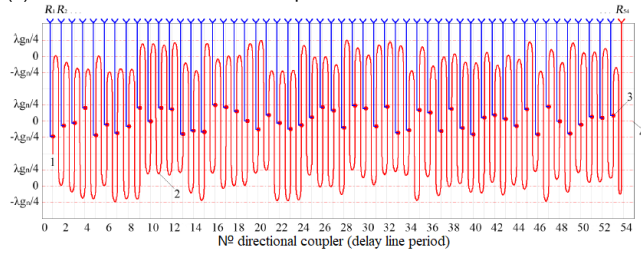


**FIGURE 14.** Structural diagram of an antenna array with an optimized geometry of the power divider.

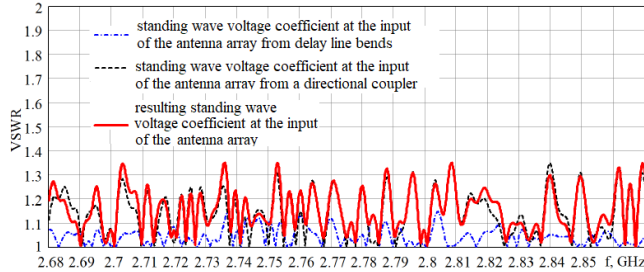


**FIGURE 15.** Standing wave ratio for voltage at the input of the antenna array after iterative optimization of the power divider geometry.

### VIII. TRANSITION TO A SERIES-PARALLEL SCHEME FOR CONSTRUCTING A POWER DIVIDER

The presented method of matching the antenna array in the operating frequency band is considered in the framework of constructing a power divider based on a delay line with a period of an *S*-shaped configuration. To implement wide-angle scanning in a relative frequency band of the order of 5% or more, a relatively dense step of installing radiators in the antenna opening is required. In this case, to ensure an adequate design of the antenna array, it is necessary to carry out the spacing of the even and odd outputs of the power divider in opposite directions relative to its center line. The period of the delay line in this case should have a *U*-shaped configuration.

By the proposed method for matching the antenna array, a violation of the periodicity of the power divider structure is required due to the displacement of the directional coupler delay line at each period and bends relative to the center line. The disadvantage of using this method with a *U*-shaped configuration of the period of the delay line (in contrast to the *S*-shaped one) is a change of up to  $\pm 90^\circ$  in the electrical length of each period, and, as a result, a violation of the linearity of the phase distribution in the opening of the antenna array. Preliminary calculations based on the given initial data show that to eliminate this shortcoming, it is advisable to make the transition from a serial scheme for

constructing a power divider to a series-parallel one (Fig. 16).

When implementing a power divider in the form of a series-parallel circuit, the length of the  $n$ -th serial period:

$$Ss_n = S + \Delta Sb_n, \quad (38)$$

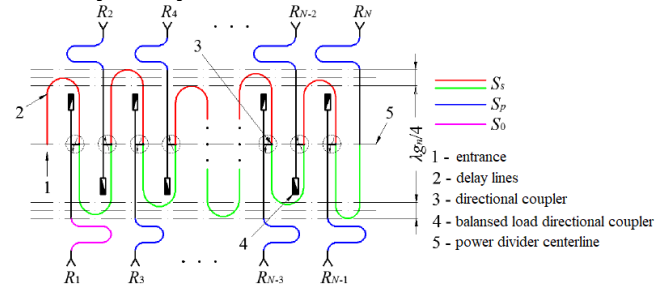
where  $\Delta Sb_n$  is the displacements of the delay line bends, found from the results of iterative optimization of the geometry of the series-type power divider.

To calculate the length of the  $n$ -th parallel period  $Sp_n$ , the expression is valid:

$$Sp_n = S_0 + \sum_{n=1}^n \Delta Sb_n, \quad (39)$$

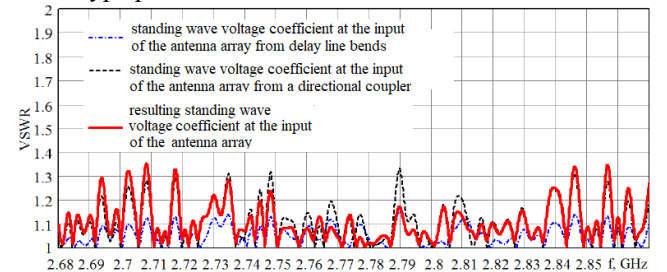
where  $S_0$  is a constant length compensating for negative values when summing delay line bend offsets  $\Delta Sb_n$ .

$\Delta Sc_n = 0$ , since the offset of the directional tap relative to the center line of the power divider, is not required, which is due to the change in the electrical length of each period of the delay line by the found distribution law  $\Delta Sb_n$ .



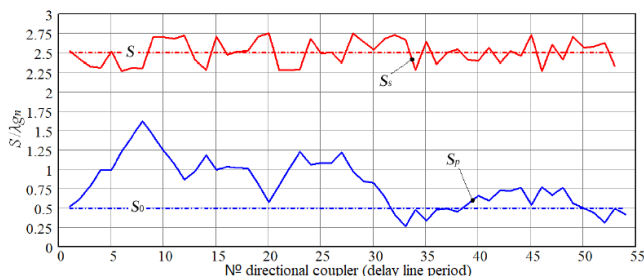
**FIGURE 16.** Structural diagram of an antenna array with serial-parallel power supply of emitters.

Fig. 17 and 18 present the results of simulation modeling of an antenna array with serial-parallel power supply of radiators (Fig. 16), obtained based on the above initial data, taking into account the offsets of the delay line bends ( $\Delta Sb_n$ ) calculated during iterative optimization of the geometry of a series-type power divider.



**FIGURE 17.** A typical implementation of the voltage standing wave ratio at the input of the antenna array with serial-parallel power supply of emitters after iterative optimization of the power divider geometry.

According to Fig. 18, it can be seen that all values of the lengths of the parallel periods  $Sp_n$  do not exceed the length of the serial period  $S$  and are within the range from  $0,25\lambda_{gn}$  to  $1,6\lambda_{gn}$ , therefore, in the practical implementation of the power divider in the form of a series-parallel circuit, a significant increase in the overall dimensions of its design is not expected. compared with the dimensions of the structure, made based on a sequential scheme.



**FIGURE 18.** Normalized lengths of serial and parallel periods of delay lines were obtained by optimizing the power divider.

## IX. CONCLUSION AND DISCUSSION

The work carried out the calculation and synthesis of antenna devices used in radio-electronic complexes on unmanned aerial vehicles. According to the provisions of the method of indefinite Lagrange multipliers, the synthesis of antenna arrays was carried out. Thus, the combined application of analytical and numerical methods of electrodynamic modeling of antenna systems on bearing surfaces makes it possible to find their realistically achievable characteristics and design parameters. The results obtained make it possible to successfully solve applied problems of developing and designing antenna systems intended for use as part of mobile radio-electronic complexes. To improve the accuracy of antenna calculation by the method of physical optics, it is proposed to use the method of multiple reflections. It is shown that with an increase in the number of re-reflections taken into account, the convergence of the result for the calculated characteristics of the antenna is observed. To test the proposed method, the same antenna was calculated using the integral equation of the electric field. The comparison showed a high degree of agreement between the results obtained by two different methods.

As a result of the research, a new method for matching an antenna array with a series or series-parallel supply of emitters was proposed. This method makes it possible to obtain an acceptable level of the voltage standing wave ratio at the input of the antenna array in the entire operating frequency band, which makes it possible to expand the antenna scanning sector without reducing the gain requirements.

## ACKNOWLEDGMENT

The authors express their deep gratitude to the entire editorial board of the journal for their professionalism and excellent work. I especially want to note the very careful and attentive attitude of the reviewers, and their detailed study of the manuscript of the article. Their comments and recommendations are constructive, which allows for improving the quality of the presented research and structuring of the article as much as possible according to the requirements of the journal. The friendly and prompt nature of communication with the editorial board contributes to the rapid resolution of all emerging issues and compliance with the stated deadlines for reviewing and publishing the article.

## REFERENCES

- [1] A.D. Tadesse, O.P. Acharya, and S. Sahu, "A Compact Planar Four-port MIMO Antenna for 28/38 GHz Millimeter-wave 5G Applications," *Advances electromagnetics*, vol. 11, no. 3, pp. 16–25, 2022. DOI: <https://doi.org/10.7716/aem.v11i3.1947>.
- [2] S. Pilytay, "Square Waveguide Polarizer with Diagonally Located Irises for Ka-Band Antenna Systems," *Advances electromagnetics*, vol. 10, no. 3, pp. 31–38, 2021. DOI: <https://doi.org/10.7716/aem.v10i3.1780>.
- [3] A. Capozzoli, C. Curcio, and A. Liseno, "CUDA-Based Particle Swarm Optimization in Reflectarray Antenna Synthesis," *Advances electromagnetics*, vol. 9, no. 2, pp. 66–74, 2020. DOI: <https://doi.org/10.7716/aem.v9i2.1389>.
- [4] A.R. Celik, and M.B. Kurt, "The Performance Comparison of a Dual-Ridge Horn Antenna and a Planar Monopole Antenna in the Microwave Breast Cancer Detection," *Advances electromagnetics*, vol. 9, no. 2, pp. 84–92, 2020. DOI: <https://doi.org/10.7716/aem.v9i2.1262>.
- [5] G. Kerim, B. Suad, "A quantized water cycle optimization algorithm for antenna array synthesis by using digital phase shifters," *International Journal of RF and Microwave Computer-Aided Engineering*, vol. 25, no. 1, pp. 21–29, 2015. DOI: <https://doi.org/10.1002/mmce.20819>.
- [6] H.I. Taisir, and M.H. Zoubir, "Array Pattern Synthesis Using Digital Phase Control by Quantized Particle Swarm Optimization," *IEEE Transactions on Antennas and Propagation*, vol. 58, no. 6, pp. 2142–2145, 2010. DOI: [10.1109/TAP.2010.2046853](https://doi.org/10.1109/TAP.2010.2046853).
- [7] P. David, O. Tamas, C.D.G. Deubauh, and K.N. Hamid, "Performance Comparison of Quantized Control Synthesis Methods of Antenna Arrays," *Electronics*, vol. 11, no. 7, pp. 994, 2022. DOI: <https://doi.org/10.3390/electronics11070994>.
- [8] V.V.S.S. Chakravarthy, P.S.R. Chowdary, D. Nihad, and A. Jaume, "Elliptical Antenna Array Synthesis using Evolutionary Computing Tools," *Arabian Journal for Science and Engineering*, vol. 47, pp. 2807–2824, 2022. DOI: <https://doi.org/10.1007/s13369-021-05852-9>.
- [9] S. Liang, T. Feng, and G. Sun, "Sidelobe-level suppression for linear and circular antenna arrays via the cuckoo search-chicken swarm optimisation algorithm," *IET Microw. Antennas Propag.*, vol. 11, pp. 209–218, 2017. DOI: <https://doi.org/10.1049/iet-map.2016.0083>.
- [10] H. Singh, B.S. Sohi, and A. Gupta, "Designing and performance evaluation of metamaterial inspired antenna for 4G and 5G applications," *Int. J. Electron.*, vol. 108, pp. 1035–1057, 2021. DOI: <https://doi.org/10.1080/00207217.2020.1819438>.
- [11] H. Singh, N. Mittal, U. Singh, and R. Salgotra, "Synthesis of non-uniform circular antenna array for low side lobe level and high directivity using self-adaptive Cuckoo search algorithm," *Arab. J. Sci. Eng.*, vol. 47, pp. 3105–3118, 2022. DOI: <https://doi.org/10.1007/s13369-021-06059-8>.
- [12] G. Yang, Y. Zhang, and S. Zhang, "Wide-band and wide-angle scanning phased array antenna for mobile communication system," *IEEE Open J. Antennas Propag.*, vol. 2, pp. 203–212, 2021. DOI: [10.1109/OJAP.2021.3057062](https://doi.org/10.1109/OJAP.2021.3057062).
- [13] R.Q. Wang, and Y.C. Jiao, "Synthesis of wideband rotationally symmetric sparse circular arrays with multiple constraints," vol. 18, pp. 821–825, 2019. DOI: [10.1109/LAWP.2019.2902565](https://doi.org/10.1109/LAWP.2019.2902565).
- [14] L. Hui, C. Yikai, and J. Ulrich, "Synthesis, Control, and Excitation of Characteristic Modes for Platform-Integrated Antenna Designs: A design philosophy," *IEEE Antennas and Propagation Magazine*, vol. 64, no. 2, pp. 41–48, 2022. DOI: [10.1109/MAP.2022.3145722](https://doi.org/10.1109/MAP.2022.3145722).
- [15] R. Castillo, R. Ma, and N. Behdad, "Platform-based electrically-small HF antenna with switchable directional radiation patterns," *IEEE Trans. Antennas Propag.*, vol. 69, no. 8, pp. 4370–4379, 2021. DOI: [10.1109/TAP.2021.3060013](https://doi.org/10.1109/TAP.2021.3060013).

- [16] Y. Liu, J. Zhang, A. Ren, H. Wang, and C. Sim, "TCM-based heptaband antenna with small clearance for metal-rimmed mobile phone applications," *IEEE Antennas and Wireless Propag. Lett.*, vol. 18, no. 4, pp. 717–721, 2019.  
DOI: 10.1109/LAWP.2019.2901808.
- [17] I.J. Islamov, E.G. Ismibayli, Y.G. Gaziyeu, S.R. Ahmadova, and R.Sh. Abdullayev, "Modeling of the Electromagnetic Field of a Rectangular Waveguide with Side Holes," *Progress in Electromagnetics Research*, vol. 81, pp. 127–132, 2019.  
DOI: 10.2528/PIERL19011102.
- [18] I.J. Islamov, N.M. Shukurov, R.Sh. Abdullayev, Kh. Kh. Hashimov, and A.I. Khalilov, "Diffraction of Electromagnetic Waves of Rectangular Waveguides with a Longitudinal," *IEEE Conferences 2020 Wave Electronics and its Application in Information and Telecommunication Systems (WECONF)*, 19806145, pp. 1–6, 01-05 June 2020,  
DOI: 10.1109/WECONF48837.2020.9131457.
- [19] A.I. Khalilov, I.J. Islamov, E.Z. Hunbataliyev, N.M. Shukurov, and R.Sh. Abdullayev, "Modeling Microwave Signals Transmitted Through a Rectangular Waveguide". *IEEE Conferences 2020 Wave Electronics and its Application in Information and Telecommunication Systems (WECONF)*, 19806152, pp. 7–14, 01-05 June 2020. DOI: 10.1109/WECONF48837.2020.9131525.
- [20] I.J. Islamov, and E.G. Ismibayli, "Experimental Study of Characteristics of Microwave Devices Transition from Rectangular Waveguide to the Megaphone," *IFAC-PapersOnLine*, vol. 51, no. 30, pp. 477–479, 2018.  
DOI: <https://doi.org/10.1016/j.ifacol.2018.11.313>.
- [21] E.G. Ismibayli, and I.J. Islamov, "New Approach to Definition of Potential of the Electric Field Created by Set Distribution in Space of Electric Charges," *IFAC-PapersOnLine*, vol. 51, no. 30, pp. 410–414, 2018. DOI: <https://doi.org/10.1016/j.ifacol.2018.11.341>.
- [22] I.J. Islamov, E.G. Ismibayli, M.H. Hasanov, Y.G. Gaziyeu, and R.Sh. Abdullayev, "Electrodynamics Characteristics of the No Resonant System of Transverse Slits Located in the Wide Wall of a Rectangular Waveguide," *Progress in Electromagnetics Research Letters*, vol. 8, pp. 23–29, 2018. DOI: 10.2528/PIERL18102904.
- [23] I.J. Islamov, E.G. Ismibayli, M.H. Hasanov, Y.G. Gaziyeu, S.R. Ahmadova, and R.Sh. Abdullayev, "Calculation of the Electromagnetic Field of a Rectangular Waveguide with Chiral Medium," *Progress in Electromagnetics Research*, vol. 84, pp. 97–114, 2019. DOI: 10.2528/PIERB19041804.
- [24] I.J. Islamov, E.Z. Hunbataliyev, and A.E. Zulfugarli, "Numerical Simulation of Characteristics of Propagation of Symmetric Waves in Microwave Circular Shielded Waveguide with a Radially Inhomogeneous Dielectric Filling," *International Journal of Microwave and Wireless Technologies*, vol. 14, no. 6, pp. 761–767, 2021. DOI: <https://doi.org/10.1017/S175907821001082>.
- [25] I.J. Islamov, M.H. Hasanov, and M.H. Abbasov, "Simulation of Electrodynamic Processes in a Cylindrical-Rectangular Microwave Waveguide Systems Transmitting Information," *11th International Conference on Theory and Application of Soft Computing, Computing with Words, Perception and Artificial Intelligence, ICSCCW – 2021*, vol. 362, pp. 246–253, 2021.  
DOI: [https://doi.org/10.1007/978-3-030-92127-9\\_35](https://doi.org/10.1007/978-3-030-92127-9_35).
- [26] I.J. Islamov, I.G. Huseynli and R. Sh Abdullayev, "Modeling of a resonator in a rectangular waveguide for transmitting electromagnetic energy," *II International Scientific Forum on Computer and Energy Sciences (WFCES-II 2021), AIP Conf. Proc.* vol. 2656, pp. 1–6, 2022. DOI: <https://doi.org/10.1063/5.0106469>.
- [27] I.J. Islamov, and M.N. Nuriyev, "Simulation of a Circular Waveguide with a Complex Structure for Transmission of Microwave Signals," *II International Scientific Forum on Computer and Energy Sciences (WFCES-II 2021), AIP Conf. Proc.* vol. 2656, pp. 7–4, 2022. DOI: <https://doi.org/10.1063/5.0106471>.
- [28] A.G. Charles, and Y. Guo, "A General Approach for Synthesizing Multibeam Antenna Arrays Employing Generalized Joined Coupler Matrix," *IEEE Transactions on Antennas and Propagation*, vol. 256, pp. 1–10, 2022. DOI: 10.1109/TAP.2022.3153037.
- [29] A.K. Amin, "A Proposed Method for Synthesizing the Radiation Pattern of Linear Antenna Arrays," *Journal of Communications*, vol. 1, no. 7, pp. 1-6, 2022. DOI: 10.12720/jcm.17.6.553–558.
- [30] A. Zeeshan, U.A.J. Zain, B. Shu-Di, and C. Meng, "Comments on "Frequency Diverse Array Beampattern Synthesis with Taylor Windowed Frequency Offsets,"". *IEEE Antennas and Wireless Propagation Letters*, vol. 21, no. 8, pp. 1713–1714, 2022.  
DOI: 10.1109/LAWP.2022.3174465.
- [31] Z. Wang, Y. Song, T. Mu, and Z. Ahmad, "A short-range range-angle dependent beampattern synthesis by frequency diverse array," *IEEE Access*, vol. 6, pp. 22664–22669, 2018.  
DOI: 10.1109/ACCESS.2018.2827079.
- [32] X. Shao, T. Hu, Z. Xiao, and J. Zhang, "Frequency Diverse Array Beampattern Synthesis with Modified Sinusoidal Frequency Offset," *IEEE Antennas Wireless Propag. Lett.*, vol. 20, no. 9, pp. 1780–1788, 2021. DOI: 10.1109/LAWP.2021.3096980.
- [33] R. Quanxin, Q. Bingyi, C. Xiaoming, H. Xiaoyu, L. Qinlong, and Z. Jiaying, "Linear Antenna Array with Large Element Spacing for Wide-Angle Beam Scanning with Suppressed Grating Lobes," *IEEE Antennas and Wireless Propagation Letters*, 21(6), 2022, 1258–1262. DOI: 10.1109/LAWP.2022.3163603.
- [34] G. Yang, Y. Zhang, and S. Zhang, "Wide-band and wide-angle scanning phased array antenna for mobile communication system," *IEEE Open J. Antennas Propag.*, vol. 2, pp. 203–212, 2021.  
DOI: 10.1109/OJAP.2021.3057062.
- [35] Y.-F. Cheng, X. Ding, W. Shao, M.-X. Yu, and B.-Z. Wang, "A novel wide-angle scanning phased array based on dual-mode pattern reconfigurable elements," *IEEE Antennas Wireless Propag. Lett.*, vol. 16, pp. 396–399, 2017. DOI: 10.1109/LAWP.2016.2580624.
- [36] M.M. Alsuyuti, E.H. Doha, S.S. Ezz-Eldien, B.I. Bayoumi, and D. Baleanu, "Modified Galerkin algorithm for solving multiplicity fractional differential equations," *Mathematical methods in the Applied Sciences*, vol. 42, no. 5, pp. 1389–1412, 2019.  
DOI: <https://doi.org/10.1002/mma.5431>.
- [37] R. Duvigneau, "CAD-consistent adaptive refinement using a NURBS-based discontinuous Galerkin method," *International Journal for Numerical Methods in Fluids*, vol. 92, no. 9, pp. 1096–1117, 2020. DOI: <https://doi.org/10.1002/flid.4819>.
- [38] M. Mazur, and J. Mazur, "Operation of the Phase Shifter Using Complex Waves of the Circular Waveguide With Periodical Ferrite-Dielectric Filling," *Journal of Electromagnetic Waves and Applications*, vol. 25, no. 7, pp. 935–947, 2011.  
DOI: <https://doi.org/10.1163/156939311795254000>.
- [39] O.P. Kusaykin, P.N. Melezhiik, A.E. Poyedinchuk, S.A. Provalov, and D.G. Seleznyov, "Surface and leaky waves of a planar dielectric waveguide with a diffraction grating," *IET Microwaves, Antennas & Propagation*, vol. 10, no. 1, pp. 61–67, 2016.  
DOI: <https://doi.org/10.1049/iet-map.2015.0158>.